International Journal of Solids and Structures 46 (2009) 3433–3440

Contents lists available at ScienceDirect

International Journal of Solids and Structures

journal homepage: www.elsevier.com/locate/ijsolstr

Analyses of crack growth along interface of patterned wafer-level Cu–Cu bonds

Viggo Tvergaard [a,*], John W. Hutchinson [b]

[a] Department of Mechanical Engineering, Solid Mechanics, Technical University of Denmark, DK-2800 Kgs. Lyngby, Denmark
[b] School of Engineering and Applied Sciences, Harvard University, Cambridge, MA 02138, USA

ARTICLE INFO

Article history:
Received 11 March 2009
Received in revised form 19 May 2009
Available online 28 May 2009

Keywords:
Interface toughness
Plasticity
Crack growth
Finite strains
Thin films

ABSTRACT

A preliminary theoretical study is carried out of the role of micron-scale patterning on the interface toughness of bonded Cu-to-Cu nanometer-scale films. The work is motivated by the experimental studies of [Tadepalli, R., Turner, K.T., Thompson, C.V., 2008b. Effects of patterning on the interface toughness of wafer-level Cu–Cu bonds. Acta Materialia 56, 438–447; Tadepalli, R., Turner, K.T., Thompson, C.V., 2008c. Mixed-mode interface toughness of wafer-level Cu–Cu bonds using asymmetric chevron test. J. Mech. Phys. Solids 56, 707–718.] wherein 400 nm Cu films were deposited in a variety of patterns on Si wafer substrates. Specimens were then produced by bringing the Cu surfaces into contact creating thermo-compression bonds. Interface toughness of these specimens was experimentally measured. The present study focuses on interface patterns comprised of bonded strips, called lines, alternating with lines of unbonded interface, all aligned parallel to the crack front. The interface toughness model employs a cohesive zone to represent separation of the interface and J_2 flow theory of plasticity to characterize the Cu films. Remote mode I loading is imposed on the elastic Si substrates. The computational model provides the resistance curve of macroscopic crack driving force versus crack advance as dependent on the work of separation and strength of the interface as well as the pattern geometry and the parameters controlling the plasticity of the Cu films. Plasticity in the Cu films makes a major contribution to the macroscopic interface toughness measured by Tadepalli, Turner and Thompson. Highlighted in this study is the difficulty of accurately representing plastic yielding in the thin films and the challenge of capturing the full range of scales in a computational model.

1. Introduction

Several experimental studies in recent years have documented the substantial enhancement of interface toughness that can arise due to patterning bonded and unbonded regions of metal-to-metal or metal-to-ceramic interfaces. Patterns with well selected geometry and scale can significantly enhance the contribution of plastic dissipation to the interface toughness (Oh et al., 1988; Litteken and Dauskardt, 2003). A revealing and thorough experimental study of these effects has been carried out by Tadepalli et al. (2008b,c) for Cu–Cu interfaces. These researchers deposited 400 nm Cu films on "thick" Si (∼mm) wafer substrates and then brought the Cu surfaces into contact and bonded them under a combination of elevated temperature and compression. On one of the wafer surfaces the Cu was patterned (as lines oriented either perpendicular to or parallel to the crack front or as square pads), while on the other wafer the Cu was deposited as a blanket film. An illustration of the cross-section of the interface for the pattern consisting of lines aligned parallel to the crack front is shown in Fig. 1. This is the pattern studied here. For reference the authors also created unpatterned interfaces having bonded blanket-to-blanket Cu films. Toughness specimens were cut from the wafer, analysed and tested under both mode I and mixed-mode conditions as described in detail in the papers cited above and in Tadepalli and Turner (2008a).

The cases studied in this paper have been chosen such that they are amenable to plane strain modelling: equally spaced lines oriented parallel to the crack front and, for reference, the unpatterned interface consisting of blanket-to-blanket films. As noted in Fig. 1, each film has thickness H and the width, D, of the bonded lines is equal to the width of the alternating unbonded lines. The thickness of the Si wafer is on the order of $1000H$; it will not appear explicitly as a parameter in our model.

In the specimens of Tadepalli et al. (2008b,c), $H = 400$ nm and, for line patterns aligned parallel to the crack front, D was varied from 25 to 250 μm. Thus, the film thickness to line width, H/D, varied from 0.016 to 0.0016. Interface separation takes place at the atomic scale and a mixed-mode cohesive zone representation of the separation process is employed in our model, characterized by a work of separation and the interface strength. Opening displacements associated with atomistic separation are on the order of 0.1 nm. Any numerical model designed to fully capture all the features influencing macroscopic interface toughness would require a mesh size less than 0.1 nm at the crack-tip and on the

* Corresponding author. Tel.: +45 4525 4273; fax: +45 4593 1475.
E-mail address: viggo@mek.dtu.dk (V. Tvergaard).

0020-7683/$ - see front matter © 2009 Elsevier Ltd. All rights reserved.
doi:10.1016/j.ijsolstr.2009.05.015

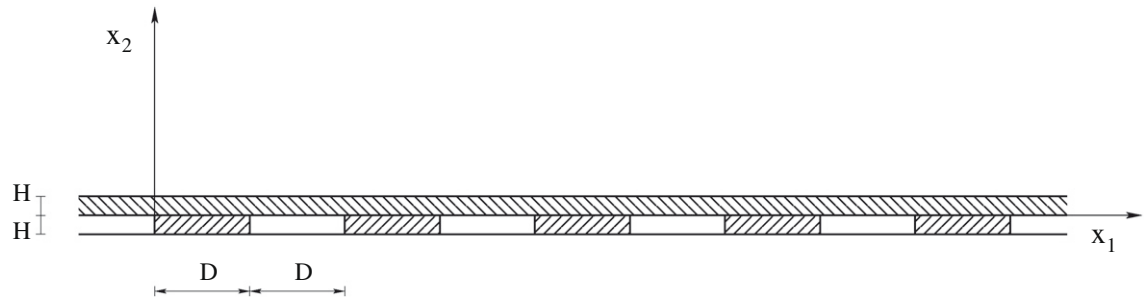

Fig. 1. Geometry near the crack-tip, where H is the Cu film thickness and D is the width of the Cu lines.

order of a fraction of a mm at the wafer scale with a relative size ratio $\sim 10^{-6}$. Moreover, detailed meshing at the intermediate scales of the film thickness and the line width would also be required. Mesh refinement spanning this range of disparate size scales is not currently feasible even for plane strain models, especially when many calculations are required to explore the role of various parameters. It is worth noting that a numerical model of interface toughness has recently been implemented that successfully links atomistic separation to the macroscopic scale through a plastic zone on the order of a micron in size (Wei and Hutchinson, 2008). However, that model had no intermediate scale associated with the line pattern width and it addressed steady-state crack growth, not the transient crack advance behaviour considered here.

In this first attempt to model the effect of micron-scale patterning on interface toughness, compromises have been made in representing the parameters characterizing both the interface cohesive zone and the plasticity of the Cu film, as described in the next section. Nevertheless, the model reveals some of the important aspects linking the macroscopic toughness to interface separation, the geometry of the interface patterning and plastic dissipation in the films. In the concluding discussion several suggestions are made for further refinements to the computational model to more realistically capture the full range of scales.

2. Problem formulation

In the present analyses only the Cu lines orthogonal to the crack growth direction (i.e., parallel to the crack front) are considered, and the analyses are carried out for plane strain conditions with the assumption of small-scale yielding under remote mode I loading conditions. As previously noted, the geometry near the crack-tip is illustrated in Fig. 1, where H denotes the film thickness and D denotes the width of the Cu lines, which is equal to the spacing of the lines. The Cu films are modelled as elastic–plastic, with the elastic properties E_1 and ν_1, a uniaxial yield stress, σ_{Y1}, and strain hardening exponent, N_1. This material is described by a finite strain generalization of J_2-flow theory (Hutchinson, 1973), with the uniaxial true stress–natural strain curve represented by a piecewise power law

$$\varepsilon = \begin{cases} \frac{\sigma}{E_1}, & \sigma \leqslant \sigma_{Y1} \\ \frac{\sigma_{Y1}}{E_1}\left(\frac{\sigma}{\sigma_{Y1}}\right)^{1/N_1}, & \sigma > \sigma_{Y1} \end{cases} \tag{1}$$

The substrate material to which the Cu films are bonded is Si, with the elastic properties E_2 and ν_2.

The substrate material is modeled as being very thick compared to both the film thickness, H, and the pattern width, D. (The widest lines in the specimens of Tadepalli et al. (2008b,c) do not meet these conditions and a more detailed representation of the substrate geometry would be required for these lines, as in the elastic analysis of Tadepalli and Turner (2008a).) A small-scale yielding approach is adopted where the stresses remote from the interface can be represented by the classical singularity field for a crack in an elastic solid:

$$\sigma_{\alpha\beta} = \frac{K_I}{\sqrt{2\pi r}} f_{\alpha\beta}(\theta) \tag{2}$$

where (r,θ) are polar coordinates. In the analyses, the associated displacements on the outer circular boundary are increased incrementally according to the singular mode I field with amplitude K_I. The relation between the energy release rate and the magnitude of the stress intensity factor is given by

$$G = \frac{1-\nu_2^2}{E_2} K_I^2 \tag{3}$$

The x_1-axis is in the crack plane and the initial crack-tip, or the edge of the first Cu line, is located at $x_1 = x_2 = 0$ (see Fig. 1). The traction–separation relation used to model the separation is specified everywhere on the interface $x_1 > 0, x_2 = 0$, at points where the Cu film on the patterned substrate is initially bonded to the upper blanket Cu film. Even though the remote loading is mode I, local asymmetry in the film geometry will usually give rise to a component of shear on the interface such that a mixed-mode interface separation model must be invoked. The traction–separation law used by Tvergaard and Hutchinson (1993) is a special version of that proposed by Tvergaard (1990) as a generalization of the model of Needleman (1987). Let δ_n and δ_t denote the normal and tangential components of the relative displacement of the crack faces across the interface in the zone where the fracture processes occur (Fig. 2). When δ_n^c and δ_t^c are critical values of these displacement components and a single separation measure is defined as $\lambda = \left[\left(\delta_n/\delta_n^c\right)^2 + \left(\delta_t/\delta_t^c\right)^2\right]^{1/2}$, the tractions drop to zero at $\lambda = 1$. With $\sigma(\lambda)$ displayed in Fig. 2, a potential from which the tractions are derived is defined as

$$\Phi(\delta_n, \delta_t) = \delta_n^c \int_0^\lambda \sigma(\lambda')\, d\lambda' \tag{4}$$

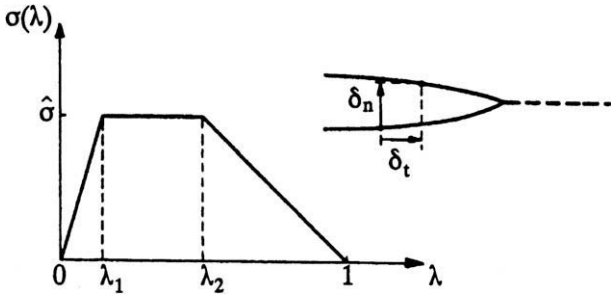

Fig. 2. Specification of traction–separation relation.

The normal and tangential components of the traction acting on the interface are given by

$$T_n = \frac{\partial \Phi}{\partial \delta_n} = \frac{\sigma(\lambda)}{\lambda}\frac{\delta_n}{\delta_n^c}, \quad T_t = \frac{\partial \Phi}{\partial \delta_t} = \frac{\sigma(\lambda)}{\lambda}\frac{\delta_t}{\delta_t^c}\frac{\delta_n^c}{\delta_t^c} \tag{5}$$

The peak normal traction under pure normal separation is $\hat{\sigma}$, and the peak shear traction is $(\delta_n^c/\delta_t^c)\hat{\sigma}$ in pure tangential separation. The work of separation per unit area of interface is given by Eq. (4) with $\lambda = 1$, and for the separation function $\sigma(\lambda)$ in Fig. 2 the work is

$$\Gamma_0 = \frac{1}{2}\hat{\sigma}\delta_n^c(1 - \lambda_1 + \lambda_2) \tag{7}$$

The work of separation in this model is independent of the mode mix, i.e. independent of the history of the normal and tangential interface displacements during separation. This is consistent with what would be expected from atomistic modeling of separation as long as positional interchanges of atoms in the surface layers do not occur. Tvergaard and Hutchinson (1992, 1993) observed that the two most important parameters characterizing the fracture process in this model are Γ_0 and $\hat{\sigma}$.

A reference stress intensity factor is defined as $K_0 = [E_2\Gamma_0/(1-\nu_2^2)]^{1/2}$ and a corresponding reference length quantity R_0, which scales with the size of the plastic zone, is defined by

$$R_0 = \frac{1}{3\pi}\left(\frac{K_0}{\sigma_{Y1}}\right)^2 = \frac{1}{3\pi}\frac{E_2\Gamma_0}{(1-\nu_2^2)\sigma_{Y1}^2} \tag{8}$$

The actual plastic zone height is an unknown, but it is larger and approximately given by $R_P \approx (K_I/K_0)^2 R_0$, as long as the plastic zone does not exceed the film thickness. To gain some perspective to the size of the plastic zone, suppose $\Gamma_0 \sim 2\,\mathrm{J\,m^{-2}}$, consistent with what might be expected from atomistic simulations and about 50% less than the smallest values measured by Tadepalli et al., and take $\sigma_{Y1} = 100$ MPa as an estimate of the yield stress of the Cu film.[1] One finds, $R_0 \sim 2\,\mu$m. Thus, the plastic zone is expected to be constrained by the elastic substrates. An important consequence of the micron scale of the plasticity is that strain gradient effects will almost certainly significantly elevate the stresses in the plastic zone and especially on the interface near the crack-tip.

Given the small Cu film thickness, $H = 400$ nm, material size effects in the form of elevation of the effective yield stress due to strain gradients are expected to be present which could be represented by using a strain gradient plasticity model. However, conventional J_2-flow theory is applied here to reduce the difficulty of the numerical problem. An additional complication is that if interface debonding between the two Cu films occurs by atomistic separation in the experiments of Tadepalli et al. (2008b), then one would expect $\delta_n^c \approx 0.5$ nm and $\hat{\sigma} \approx 10$ GPa consistent with a work of separation, $\Gamma_0 \sim 2\,\mathrm{J\,m^{-2}}$. In the numerical implementation, values of δ_n^c as small as 0.5 nm together with the much larger values of the Cu line dimensions D and H would require meshing refinements that are not computationally feasible. Moreover, the largest stresses that can act on an interface when conventional plasticity is used to characterize the Cu films is on the order of 4–$5\sigma_{Y1}$ and thus interfaces with strengths as large as $\hat{\sigma} \approx 10$ GPa would never fail according to any models based on conventional J_2 plasticity (Tvergaard and Hutchinson, 1992).

It is clear from the above discussion that compromises must be made in choosing the material parameters in the computational model, as will be evident in the parameter ranges used in the computations described below.

[1] A yield stress of the Cu films was not reported. $\sigma_{Y1} = 100$ MPa can be considered as representative, but gradient effects and the small thickness of the films are expected to elevate the effective flow stress of the Cu, as discussed further.

3. Numerical method

A Lagrangian convected coordinate formulation of the field equations is used, with a material point identified by the coordinates x_i in the reference configuration, accounting for finite strains. The contravariant components of the Cauchy stress tensor σ^{ij} and the Kirchhoff stress tensor τ^{ij} are related by $\tau^{ij} = \sqrt{G/g}\sigma^{ij}$. The metric tensors in the current and reference configurations are denoted by G_{ij} and g_{ij}, with the determinants G and g, respectively, and the incremental stress-strain relationship is of the form $\dot{\tau}^{ij} = L^{ijkl}\dot{\eta}_{kl}$, where L^{ijkl} are the instantaneous moduli.

The Lagrangian strain tensor is given by

$$\eta_{ij} = \frac{1}{2}\left(u_{i,j} + u_{j,i} + u^k_{,i}u_{k,j}\right) \tag{9}$$

where u^i are the displacement components on the reference base vectors and $(\,)_{,j}$ denotes covariant differentiation in the reference frame. Numerical solutions are obtained by a linear incremental solution procedure, based on the principle of virtual work

$$\int_V \tau^{ij}\delta\eta_{ij}\,dV + \int_{S_I}\{T_n\delta(\delta_n) + T_t\delta(\delta_t)\}dS = \int_S T^i\delta u_i\,dA \tag{10}$$

Here, V and A are the volume and surface of the body in the reference configuration, respectively, S_I is the interface surface region where the two Cu films are in contact, and T^i are contravariant components of the nominal surface tractions. An incremental version of the PVW (10) is used for the numerical solution. The displacement fields are approximated in terms of planar 8-noded isoparametric plane strain elements. The volume integral in Eq. (10) is carried out by using 2×2 integration points within each element.

A circular region with radius A_o is analyzed numerically. Fig. 3 illustrates the initial near-tip mesh in the centre of the region analyzed, with 100×4 uniform quadrilaterals on each side of the interface in the range where crack growth is studied. The length of one square element inside the uniform mesh is denoted Δ_0, and the initial crack-tip is located at $x_1 = 0$. The outer radius is chosen to be $A_0 = 2000H = 8000\Delta_o$. In all the cases analyzed, the load is applied on the outer boundary in the form of the displacements of the elastic singularity field.

4. Results

To obtain modeling results as realistic as possible given the constraints noted in Section 2, the yield strength of the copper is taken to be larger than feasible even for a very thin film, while the strength of the interface is taken to be somewhat lower than what might be expected for atomistic separation of a Cu–Cu interface. Specifically, the analyses of crack growth carried out here take the Cu film and the Cu lines to be represented as an elastic-plastic material with $\sigma_{Y1}/E_1 = 0.02$, $\nu_1 = 0.33$ and $N_1 = 0.25$. For Cu with $E_1 = 130$ GPa, this corresponds to $\sigma_{Y1} = 2.6$ GPa. The Si outside the Cu films is taken to have elastic properties specified by $E_2/E_1 = 1.34$ and $\nu_2 = 0.2$. In the traction–separation law the values $\delta_n^c/\delta_t^c = 1$, $\delta_n^c = 0.1H = 0.4\Delta_0$, $\lambda_1 = 0.15$ and $\lambda_2 = 0.50$ are used, while $\hat{\sigma}/\sigma_{Y1}$ is varied with values as large as 3. Thus, the strongest interfaces considered here have $\hat{\sigma} = 7.8$ GPa which could conceivably be representative of atomistic separation. From (7), it is seen that $\Gamma_0 \sim 200\,\mathrm{J/m^2}$ based on the values above used in the model for interfaces having $\hat{\sigma} = 7.8$ GPa and $\delta_n^c = 0.1H = 40$ nm. Thus, the work of separation of the interface exceeds what should be expected from atomistic considerations by about a factor of 100. It can be noted that compromises in material parameter selection to circumvent the problem of interface separation in the presence of plasticity in fundamental studies of interface toughness are not unique to this paper. For example, O'Day et al. (2006) used much lower interface

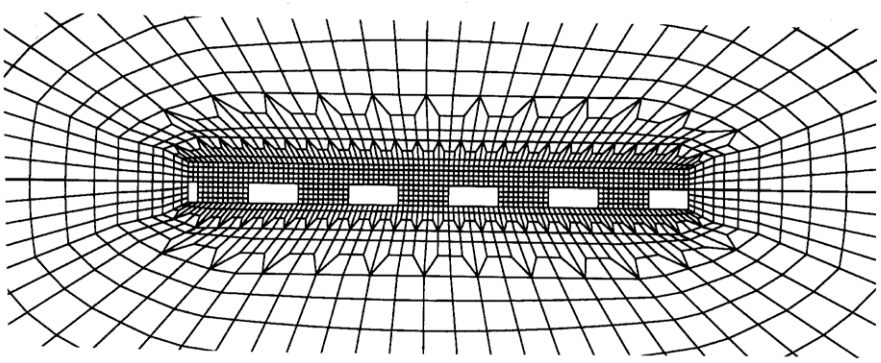

Fig. 3. Mesh used for some of the crack growth analyses for $D/H = 2.5$. The upper half of the fine mesh region has the thickness H of the Cu film, and the lower half of the fine mesh region represents the cross-sections of the first five Cu lines.

strength in their model than would be expected from atomistic considerations.

Resistance curves for a semi-infinite width of the Cu line are shown in Fig. 4. The initial crack front coincides with a 90° edge on the Cu substrate with only bonded region ahead ($D/H \to \infty$). The uniform mesh region in the two Cu films consists of 100×8 elements, so that the length of a square element in the uniform mesh is $\Delta_0 = 0.25H$. The energy release rate G according to (3) is plotted as a function of the amount of crack growth Δa, normalized by Γ_0 and R_0, respectively. Here, Δa denotes the value (values) of the x_1 coordinate at the current crack-tip (tips) defined as the point of full separation of the crack surfaces (i.e. $\lambda \geqslant 1$). The resistance curve for $\hat{\sigma}/\sigma_{Y1} = 2.0$ shows a high peak as the crack initiates from the 90° edge on the Cu substrate and subsequently the toughness decays to a stable steady-state level slightly elevated above the atomistic work of separation Γ_0. In this case the scaling length of the plastic zone is $R_0/H = 0.999$, corresponding to $R_0/\Delta_0 = 3.99$. For comparison, the figure also shows a purely elastic result with an initial peak lower than that for the elastic-plastic Cu films and a steady-state toughness which is precisely Γ_0. Thus, with $\hat{\sigma}/\sigma_{Y1} = 2.0$, there is a small burst of plastic dissipation associated with the early stage of growth, but virtually none after crack advance of about $5R_0$. Results for two higher values of the debonding peak stress, $\hat{\sigma}/\sigma_{Y1} = 2.5$ and $\hat{\sigma}/\sigma_{Y1} = 3.0$, respectively, are also shown in Fig. 4. In these cases the reference size of the plastic zone is larger, with the values $R_0/H = 1.25$ and $R_0/H = 1.50$, respectively. An important feature of these curves is that the first separation of the interface does not occur at the edge of the bonded region. Instead, the first separation occurs in the interior of the Cu bond region at the location of the peak of G. From this point, one crack-tip grows backwards until it reaches the edge of the bonded region while the other tip grows forwards until it attains steady state when $\Delta a \approx 5R_0$.

The resistance curves for the semi-infinite bonded films in Fig. 4 reveal several essential aspects of the toughening effect. First, higher values of $\hat{\sigma}/\sigma_{Y1}$ give rise to higher initial peak values of the fracture toughness and also to higher values of the steady-state toughness. Steady-state conditions are attained after the crack has advanced several times R_0. For $\hat{\sigma}/\sigma_{Y1} = 3$, the steady-state toughness is approximately 50% higher than the atomistic work of separation. Another feature revealed by Fig. 4 is that even the elastic film has an initial peak with G greater than Γ_0. This peak is due to the fact that the region surrounding the interface is more compliant when the crack first begins to advance—in effect, the crack is initiated from a slightly blunted notch. Higher remote loads must be applied to reach the stresses required for separation. This effect is compounded when

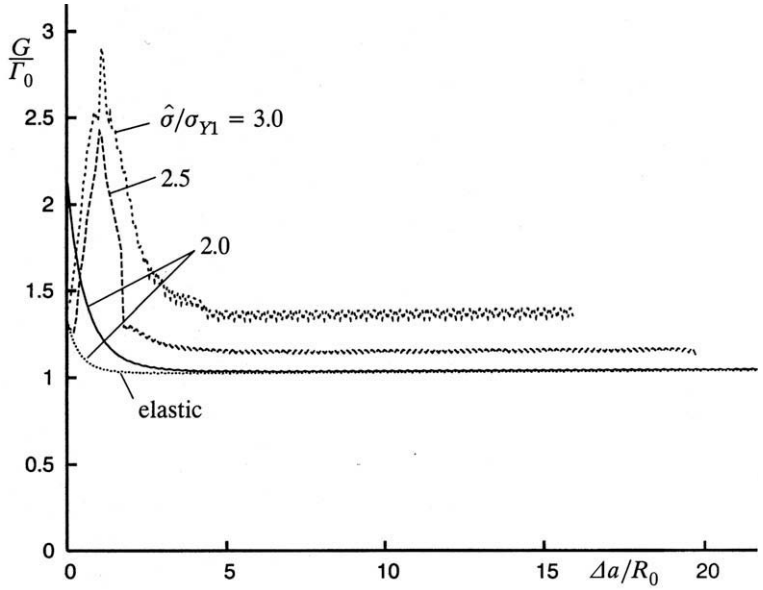

Fig. 4. Crack growth resistance curves for a single Cu line (D/H is large), for three values of the interface strength $\hat{\sigma}/\sigma_{Y1}$. The elastic curve included for comparison neglects plasticity in the Cu films.

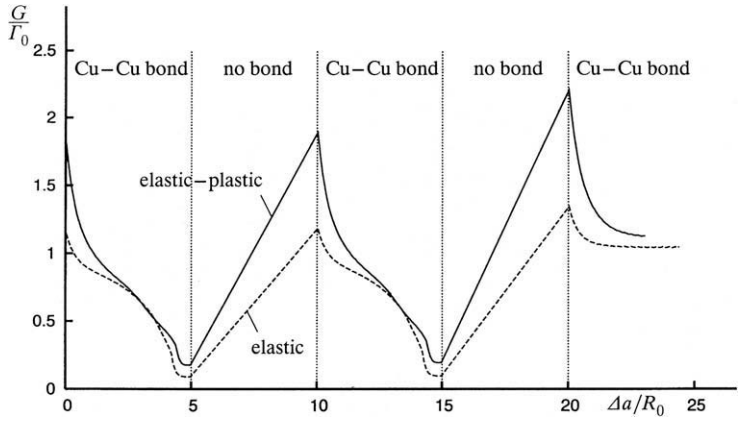

Fig. 5. Crack growth resistance curve for the Cu line width $D/H = 5$, with the interface strength $\hat{\sigma}/\sigma_{Y1} = 2.0$. The elastic curve included for comparison neglects plasticity in the Cu films. Only the first two Cu lines are fully represented in the mesh, with a uniform 20×4 mesh on each cross-section. Straight line segments are drawn to connect bonded lines across an unbonded region.

the films deform plastically because the plasticity is significantly less constrained when the tip is at the edge than when the tip has advanced. This is also closely related to why separation initiates at an interior point of the interface rather than at the edge when $\hat{\sigma}/\sigma_{Y1}$ becomes large enough.

Fig. 5 applies to alternating bonded ($\hat{\sigma}/\sigma_{Y1} = 2.0$) and unbonded lines with $D/H = 5$. It also shows a dashed curve obtained by assuming that the thin Cu films are elastic, with no plastic yielding. All other parameter values are identical to those for the elastic–plastic curve and the value R_0 used for normalization is that corresponding to the elastic–plastic curve. This elastic curve makes it clear that plasticity in the Cu films adds significantly to the crack growth resistance, particularly each time crack growth initiates at a new Cu line. Crack growth resistance for both the elastic and the elastic–plastic Cu films falls below Γ_0 when the crack has traversed only about 1/3 the distance across the bonded line. At this point, the leading front of the cohesive zone has already advanced beyond the right edge of the line significantly elevating the local net section stress. It is noted that for each of the two curves the last peak value shown is unrealistically large since the Cu line pattern is only represented numerically inside the uniform mesh region, and thus the last peak refers to the initiation of crack growth in a line of infinite width.

Fig. 6 shows resistance curves for $D/H = 5$ as in Fig. 5. The three different curves correspond to the same three values of $\hat{\sigma}/\sigma_{Y1}$ considered in Fig. 4, and the curve for $\hat{\sigma}/\sigma_{Y1} = 2.0$ is identical to that shown in Fig. 5. Both the meshes and all other parameters than $\hat{\sigma}/\sigma_{Y1}$ are identical for the three computations. It is seen that the minima and the maxima occur at a slightly smaller value of $\Delta a/R_0$ when the value of $\hat{\sigma}/\sigma_{Y1}$ is larger, because the corresponding reference size of the plastic zone R_0 is larger. As in the case of the semi-infinite bond, first separation at the peak values of G occur at an interior point of the bonded line at the higher values of $\hat{\sigma}/\sigma_{Y1}$. Here, and in subsequent figures, when first separation occurs in the interior of a line, we have not plotted the backward growth of the crack-tip from the peak of G. Instead, a straight line is drawn between the two points on the resistance curve where the crack front jumps across the "no bond" region from one bonded Cu line to the peak of the next where debonding initiates. The effect of interface strength $\hat{\sigma}$ on increasing plastic dissipation and crack growth resistance is evident in this figure.

This point is further illustrated by the deformed meshes in Fig. 7 for the case of $\hat{\sigma}/\sigma_{Y1} = 3.0$ in Fig. 6, at two stages debonding. Cracking of the interface of these Cu lines has started in the interior of the interface, spreading backwards and forward to the two edges of the line. Considerable plastic deformation is obvious. Thin

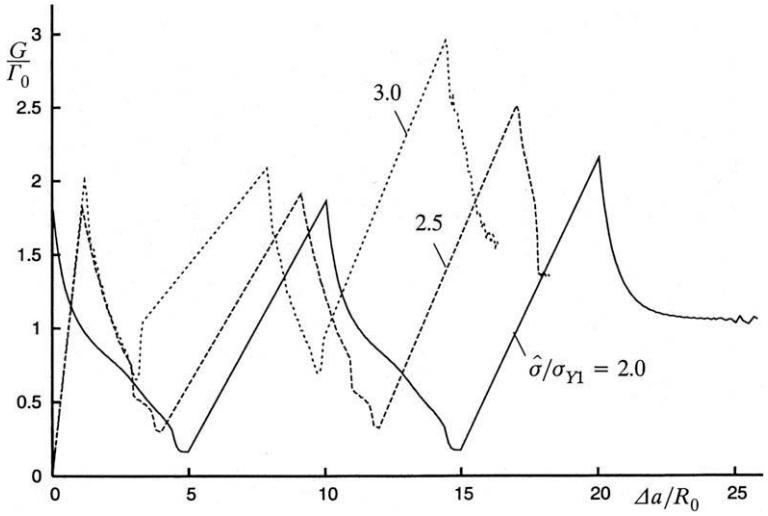

Fig. 6. Crack growth resistance curves for the Cu line width $D/H = 5$, for three values of the interface strength $\hat{\sigma}/\sigma_{Y1}$. Only the first two Cu lines are fully represented in the mesh, with a uniform 20×4 mesh on each cross-section.

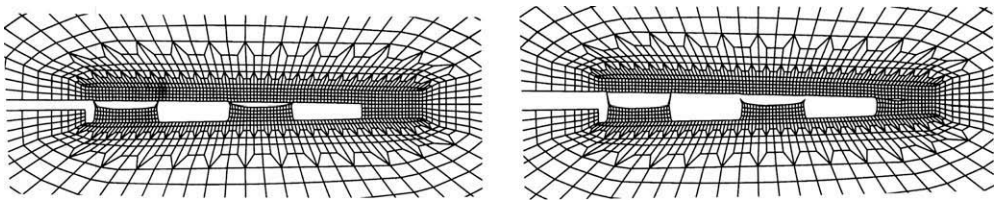

Fig. 7. Deformed meshes at two stages of crack growth, with the interface strength $\hat{\sigma}/\sigma_{Y1} = 3.0$ and the Cu line width $D/H = 5$. Only the first two Cu lines are fully represented in the mesh. Cracking of a Cu line does not start at the edges.

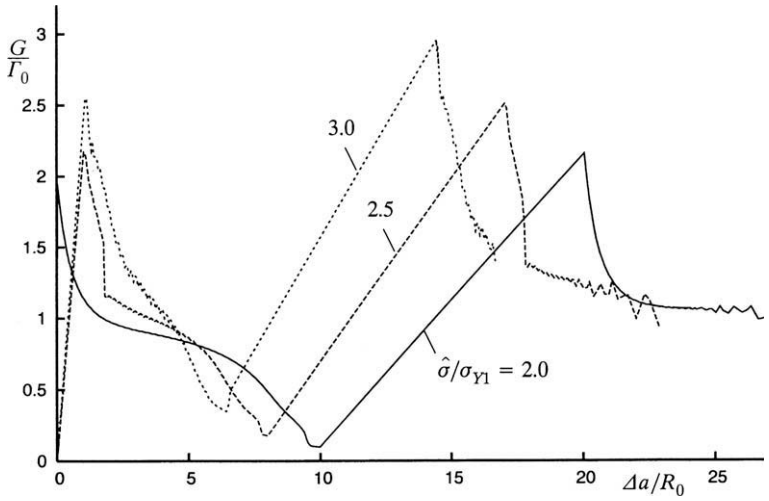

Fig. 8. Crack growth resistance curves for the Cu line width $D/H = 10$, for three values of the interface strength $\hat{\sigma}/\sigma_{Y1}$. Only the first Cu line is fully represented in the mesh, with a uniform 40×4 mesh on each cross-section.

bridges of Cu form at the edges of the line in the final stages of separation, and the numerical solution is not able to accurately represent the final failure at the bridges. In reality, the bridges would fail by necking and tearing but the mesh used is not fine enough to accurately resolve this behavior.

Fig. 8 shows crack growth resistance curves for $D/H = 10$ analogous to those in Fig. 6. The main difference here is that the crack growth resistance remains above Γ_0 for crack advances to approximately $\Delta a \cong 5R_0$, at which point the leading front of the cohesive zone begins to interact with the right edge of the bonded line. This observation is consistent with the fact that the length of the cohesive zone scales with the length

$$c = E\Gamma_0/\hat{\sigma}^2 \tag{11}$$

as can be readily established from the well known Dugdale-Barenblat model. The results of Figs. 5, 6 and 8 suggest that the width of the cohesive zone is roughly 4–5c since c from (11) is in the range from 200 to 400 nm. Thus, the sets of results for $D/H = 5$ and $D/H = 10$ are dominated by the interaction between the cohesive zone and the right edge of the bonded regions except during the first stage when the crack first begins to grow. The first stage is similar to that for the semi-infinite case in Fig. 4. The other difference here compared to Fig. 6 is that with the increased aspect ratio of the cross-section of the Cu line and the same 100×4 uniform mesh on each side of the interface only the first Cu line can be fully represented numerically and already the second peak on the curves refers to the initiation of crack growth in a line of infinite width.

In Fig. 9 three crack growth resistance curves are compared for three different line widths, all with $\hat{\sigma}/\sigma_{Y1} = 3.0$. The curves for the two smaller values of D/H have already been shown in Figs. 6 and 8. The additional curve for $D/H = 20$ is computed by using 80×4 elements on the cross-section of the line, so that only one Cu line could be represented inside the mesh applied. The first part of the curve for $D/H = 20$, until $\Delta a/R_0 \approx 8$, is practically identical with the curve for $\hat{\sigma}/\sigma_{Y1} = 3.0$ in Fig. 4, indicating that there is initially no interaction with the right edge of the Cu line. The end of the curve shown, after the minimum, is the point at which next separation will occur in the following Cu line.

For $\hat{\sigma}/\sigma_{Y1} = 2.0$ the curves in Figs. 6 and 8 have been recomputed using a cruder mesh, with 100×2 uniform quadrilaterals on each side of the interface in the crack growth range, so that there are only two elements through the thickness of a Cu line, and $\Delta_0 = 0.5H$. This allows for numerical representation of a larger number of Cu lines. The initial peaks show rather good agreement between the predictions obtained for the two meshes, but the peaks around $\Delta a/R_0 = 20$ are not unrealistically high for the cruder mesh, as the Cu line starting here is not the last Cu line represented numerically. Similar cruder mesh computations have also been carried out for the curves in Figs. 6 and 8 with $\hat{\sigma}/\sigma_{Y1} = 3.0$. Here the agreement is slightly less good, as there is more localized plasticity, which is more accurately represented by the finer mesh.

Crack growth resistance curves have also been calculated for $D/H = 2.5$, i.e. for the small aspect ratio Cu lines illustrated by the initial mesh in Fig. 3. Here, several Cu lines are represented numerically, but otherwise the curves found for the lower values of $\hat{\sigma}/\sigma_{Y1}$ are rather similar to those found in Figs. 6 and 8.

5. Discussion

In this paper attention has been focused the crack growth resistance of patterned Cu–Cu interfaces with alternating lines of bonded and unbonded regions aligned parallel to the crack front. Two distinct contributions of plastic dissipation to the crack growth resistance have been highlighted by the model. One contribution is

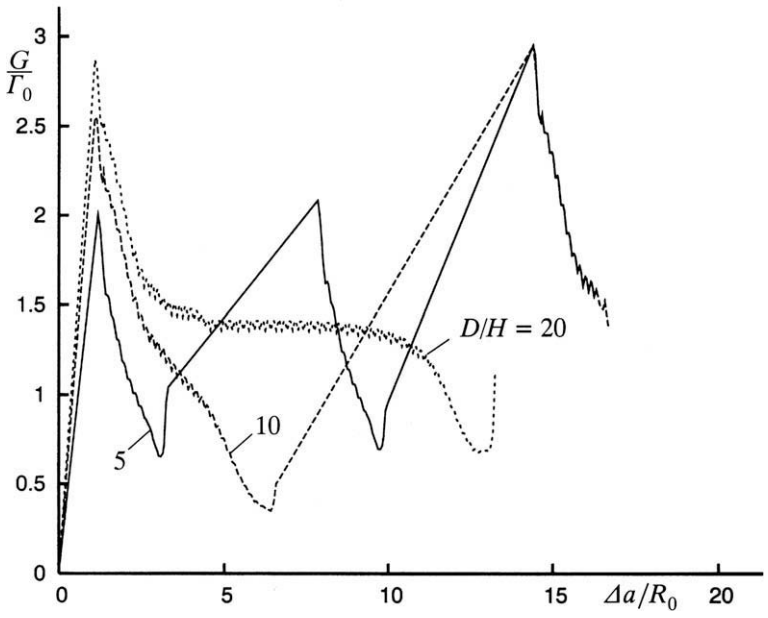

Fig. 9. Crack growth resistance curves for $\hat{\sigma}/\sigma_{Y1} = 3.0$, for three values of the Cu line width D/H. Each Cu line is represented by a uniform mesh, with 20×4, 40×4 and 80×4 elements, respectively, on each cross-section.

associated with steady-state crack-tip plasticity that does not depend on patterning. The other is directly related to the patterning: it is transient and associated with enhanced plastic deformation each time debonding is initiated as the interface crack encounters a new line.

Two material length parameters are relevant to these effects. The length (8) that scales the size of the plastic zone,

$$R_0 = \frac{1}{3\pi}\frac{E_2\Gamma_0}{(1-\nu_2^2)\sigma_{Y1}^2},$$

and the length (11) that scales the length of the cohesive zone of the advancing crack-tip

$$c = \frac{E_2\Gamma_0}{\hat{\sigma}^2}$$

Steady-state crack growth within a line of width D can occur if $D \gg R_0$ and $D \gg c$. If D meets these conditions, steady-state crack growth resistance will prevail when the advancing crack-tip is within the line interface at distances that are simultaneously greater than several times R_0 from both edges of the line and at a distance greater than about $5c$ from the right edge of the line. The requirement related to R_0 ensures that the plastic zone does not interact with either edge of the line, while that related to c ensures that the cohesive zone does not interact with the right edge of the line. Transient effects occur when either, or both, of these requirements fail to hold. Transient effects are also associated with the blunt notch at the left edge of each line, set by the thickness of the film, as illustrated by the resistance curves for the elastic films in Figs. 4 and 5.

Steady-state crack growth resistance is strongly dependent on the interface strength through the dimensionless parameter $\hat{\sigma}/\sigma_{Y1}$. For $\hat{\sigma}/\sigma_{Y1} < 2$, there is little plastic dissipation in steady-state growth, but the crack growth resistance increases sharply with increasing $\hat{\sigma}/\sigma_{Y1}$ above 2. As has been emphasized in the body of the paper, the trends revealed by the present model are realistic when presented in terms of the dimensionless ratio, G/Γ_0, but absolute quantitative predictions would require the incorporation of a plasticity theory in the model that is more accurate at the small scale dictated by the thickness of the Cu films and finer meshing associated with much smaller values of δ_n^c.

The most important transient effect occurs as the advancing crack-tip encounters a new line and reinitiates separation, either at the edge of the line or near the edge in the interior depending on the magnitude of $\hat{\sigma}/\sigma_{Y1}$. A significant "hump" of plastic dissipation is associated with this transient and it persists for a crack advance that scales with R_0—it can be many times R_0 if $\hat{\sigma}/\sigma_{Y1} \geqslant 3$. Thus, the effective toughness of the interface can be enhanced by patterning by choosing the line width, D, relative to R_0 such that the transient dissipation humps comprise a significant contribution to the total plastic dissipation. Transient behavior also occurs when the cohesive zone at the crack-tip interacts with the right end of the line, as illustrated in Figs. 5 and 6. However, the present model almost certainly misses the importance of this effect due to the difficulty of numerically modeling realistic combinations of material and geometric parameters, as noted in the body of the paper. In the examples in Figs. 5 and 6 the length of the cohesive zone is a finite fraction of the line width, D, whereas in more realistic systems, such as those of Tadepalli et al. (2008b), c is expected to be a tiny fraction of D, as discussed further below.

To relate the experimental results of Tadepalli et al. (2008b) for orthogonal Cu lines to the present theoretical predictions their toughness measurements must be interpreted. Stable crack growth in the chevron specimens begins prior to attainment of a smooth peak load followed by a gradually decreasing load giving way to abrupt failure. The toughness is identified with the energy release rate associated with the peak load. For the orthogonal lines, we assume that the measured toughness reflects the combined energy of separation and plastic dissipation associated with the crack front traversing a single line. This is consistent with the fact that for broad lines ($D/H \geqslant 200$) the reported experimental toughness is essentially identical to that for interfaces with blanket films. In their toughness plots, Tadepalli et al. do not correct the toughness of the interfaces with orthogonal lines to account for the fact that only one half of the surface area is bonded, consistent with the assumption that the crack-tip is sampling only one line. If the toughness were associated with the tip traversing multiple broad lines, then it should be approximately one half that for the interface with blanket films.

The measured toughness of the interfaces with blanket films or broad orthogonal lines is approximately $G_C = 2.5\ \mathrm{J/m^2}$, which falls

within the range that one would expect for an interface failing by atomic separation accompanied by some plastic dissipation. However, it is not clear from micrographs of the fracture surface presented by Tadepalli et al. that atomistic separation is the governing mechanism at least for some of the cases. Void nucleation, growth and coalescence seem evident for some of the narrowest patterns with high toughness. As noted above, lines with $D/H \geqslant 200$ have a measured toughness comparable to blanket films. For lines with $D/H \cong 150$ the toughness is about $5\,\mathrm{J/m^2}$, while it increases to almost $15\,\mathrm{J/m^2}$ for $D/H \cong 25$. The experimental trend for the interface patterned by square pads of dimension $D \times D$ is very similar because Tadepalli et al. multiplied the measured toughness by a factor of 2 to account for the fact only 1/2 of the crack front encounters a bonded interface.

If one assumes that interface separation associated with the mode I data acquired by Tadepalli et al. (2008b) is governed by atomic separation, then one would expect interface strengths on the order of $\hat{\sigma} \sim 10\,\mathrm{GPa}$, separation displacements on the order of $\delta_n^c \sim 0.1\,\mathrm{nm}$, and a work of separation $\Gamma_0 \sim 1\,\mathrm{J\,m^{-2}}$. The first two parameters are not known for the Tadepalli et al. data, but, as just noted, a work of separation of the Cu–Cu interface on the order of $\Gamma_0 \sim 1\,\mathrm{J\,m^{-2}}$ is consistent with their data. Based on these parameters, the length parameter c that scales the length of the cohesive zone is $c \sim 1\,\mathrm{nm}$ and this too is consistent with atomistic separation. As noted earlier, the yield stress of the Cu films has not been determined. If $\sigma_{Y1} = 100\,\mathrm{MPa}$, then $R_0 \cong 1\,\mu\mathrm{m}$, while if $\sigma_{Y1} = 300\,\mathrm{MPa}$, then $R_0 \cong 100\,\mathrm{nm}$. Because that the plastic zone size is $R_P \cong (G/\Gamma_0)R_0$, it seems likely that the plastic zone is on the order of the film thickness during crack propagation in the specimens of Tadepalli et al., especially for the toughest interfaces.

Tadepalli et al. (2008c) have shown SEM micrographs and AFM images of Cu–Cu fracture surfaces to illustrate that the fracture surfaces are much rougher under mixed-mode loading where plasticity plays a larger role. This effect of plasticity is also illustrated in (Tadepalli et al., 2008b) by SEM micrographs for sufficiently small pattern size of orthogonal lines or pads. This is likely to mean that when plasticity gains increasing importance for decreasing width of the Cu lines also the parameter values for the cohesive zone model should be gradually changed. When debonding involves plastic mechanisms, as e.g. void growth to coalescence, leading to very rough fracture surfaces the work of separation per unit area is much larger than for atomic separation. This change would involve a much larger increase of the critical normal separation δ_n^c than the corresponding reduction of the critical peak stress $\hat{\sigma}$. Such changes of the debonding parameters are not included in the present computations.

In light of the behavior brought out by the present model, the following understanding emerges for the increasing toughness of the experimental data with decreasing line width for orthogonal lines as observed by Tadpelli et al. The toughness enhancement is due to a combination of plastic dissipation associated with the initiation of debonding for each line and the subsequent steady-state plastic dissipation when the crack-tip is not interacting with the line edges. When the ratio of interface strength to yield stress, $\hat{\sigma}/\sigma_{Y1}$, is sufficiently high, both contributions can be significant. If patterning is to control the enhancement, as is clearly seen for the experiments of Tadpelli et al. when $D/H < 150$, the line width must be such that the transient hump of dissipation comprises the dominate plasticity contribution.

Finally, as noted in the body of the paper, it remains to carry out computations with this type of model for more realistic values of the parameters controlling interface separation and with a plasticity theory more capable of representing the strong size dependence known to arise at the scale set by the thin films. Based on the findings here, we believe that a study that focused on initiation and the transition to steady-state behavior in a single line would be feasible, even with exceptionally fine meshing that would be required.

The problems addressed in this paper clearly represent a challenge in bridging across scales from the macroscopic down to level of atomistic separation. As noted above, we believe that some simulation aspects are within reach using existing methods. However, if high accuracy numerical resolution is required at an intermediate scale set by the pattern of the thin film, then it seems likely that more advanced multi-scale numerical methods will be needed.

References

Hutchinson, J.W., 1973. Finite strain analysis of elastic–plastic solids and structures. In: Hartung, R.F. (Ed.), Numerical Solution of Nonlinear Structural Problems. ASME, New York, p. 17.

Litteken, C.S., Dauskardt, R.H., 2003. Adhesion of polymer thin-films and patterned lines. Int. J. Fracture 119, 475–485.

Needleman, A., 1987. A continuum model for void nucleation by inclusion debonding. J. Appl. Mech. 54, 525–531.

O'Day, M.P., Nath, P., Curtin, W.A., 2006. Thin film delamination: a discrete dislocation analysis. J. Mech. Phys. Solids 54, 2214–2234.

Oh, T.S., Rödel, J., Cannon, R.M., Ritchie, R.O., 1988. Ceramic/metal interfacial crack growth: toughening by controlled microcracks and interfacial geometries. Acta Metall. 36, 2083–2093.

Tadepalli, R., Turner, K.T., 2008a. A chevron specimen for the measurement of mixed-mode interface toughness of wafer bonds. Eng. Fracture Mech. 75, 1310–1319.

Tadepalli, R., Turner, K.T., Thompson, C.V., 2008b. Effects of patterning on the interface toughness of wafer-level Cu–Cu bonds. Acta Mater. 56, 438–447.

Tadepalli, R., Turner, K.T., Thompson, C.V., 2008c. Mixed-mode interface toughness of wafer-level Cu–Cu bonds using asymmetric chevron test. J. Mech. Phys. Solids 56, 707–718.

Tvergaard, V., 1990. Effect of fibre debonding in a whisker-reinforced metal. Mater. Sci. Eng. A 125, 203–213.

Tvergaard, V., Hutchinson, J.W., 1992. The relation between crack growth resistance and fracture process parameters in elastic–plastic solids. J. Mech. Phys. Solids 40, 1377–1397.

Tvergaard, V., Hutchinson, J.W., 1993. The influence of plasticity on mixed mode interface toughness. J. Mech. Phys. Solids 41, 1119–1135.

Wei, Y., Hutchinson, J.W., 2008. Toughness of Ni/Al203 interfaces as dependent on micron-scale plasticity and atomistic-scale separation. Philos. Mag. 88, 3841–3859.